08,02

Evolution of leakage currents in the $BiFeO_3/TiO_2$(Nt)/Ti structure during short-term switching from high to low voltage

© G.M. Gajiev, Sh.M. Ramazanov¶, R.Z. Zeynalov, T.N. Efendieva, N.S. Abakarova

Amirkhanov Institute of Physics, Daghestan Federal Research Center,
Russian Academy of Sciences,
Makhachkala, Russia

¶ E-mail: ramazanv@mail.ru

Received November 15, 2025
Revised November 21, 2025
Accepted December 2, 2025

This work the influence of the magnitude and duration of preliminary polarizing voltage on the relaxation currents and current–voltage characteristics of the $BiFeO_3/TiO_2$(Nt)Ti structure was studied. A two-stage scheme was used: preliminary polarization $U_{pol} = 30-55$ V ($t_{pol} = 0.1-4$ sec) followed by a measurement voltage $U_{meas} = 0.1-2$ V, within which the relaxation currents $J(t)$ were recorded. It was shown that the $I(t)$ dynamics and the shape of the $J-V$ characteristics are significantly modified by the parameters U_{pol} and t_{pol}; current maxima, sign inversion at low voltages, and N-shaped $I-V$ characteristics were observed. Analysis of the dependences in Schottky, Poole–Frenkel, and space-charge-limited current coordinates revealed the dominant contribution of Schottky and space-charge-limited current mechanisms. The trap-filling voltage was used to estimate the concentration of oxygen vacancies, which increases with higher U_{pol}, consistent with the drift and accumulation of $V\ddot{o}$ near the cathode. The results demonstrate that controlled preliminary polarization allows for the targeted modification of the structure's conductivity and the optimization of operating regimes for memristive elements based on $BiFeO_3$.

Keywords: $BiFeO_3$, leakage current, nanotubes, thin films, memristor.

DOI: 10.61011/PSS.2026.01.63250.325-25

1. Introduction

Recently, metal-dielectric (semiconductor)-metal structures have again attracted the attention of researchers around the world after the proclamation of the concept of a memristor crossbar as an alternative to the von Neumann architecture [1–3]. Memristor (nanoscale memory element between two electrodes) crossbar — a system of parallel nanowires intersecting another such system at an angle, where memristors themselves are located in the nodes between the contacts [3]. Thanks to the memristor's ability to simultaneously exhibit the properties of a non-volatile storage device, a logic device, and a high-speed switch, it has become possible to manufacture a new generation processor in which the problem of the von Neumann bottleneck effect is easily avoided.

Among the thin-film oxides of transition metals seen as promising materials for memristor manufacturing, a semiconductor (dielectric) $BiFeO_3$ (BFO) plays a special part. In addition to its outstanding multiferroid properties, BFO has previously demonstrated the properties of resistive switching [4,5]. A number of studies have shown that buffer layers (in particular, an array of TiO_2 nanotubes) can be used to enhance the magnetoelectric effect and increase the effective film area, as well as improve the electrophysical and electrochemical properties of BFO-based films, which expands the possibilities of practical application of these materials [6–9].

Relaxation currents that occur in thin-film ferroelectrics immediately after switching on/off the voltage have a significant effect on the operation of memory elements, strongly depend on the processes of polarization and depolarization, sometimes leading to a noticeable modification of $I-V$-dependencies. The relaxation time defined from the dependence $I(t)$ after voltage supply/relief on the sample is an important parameter of active dielectrics. Its value depends on the extent of the material structure perfection, the presence of the current carrier shallow traps and the state of the interface of the film structure phases, and may reach the values from fractions of a second to several minutes. Therefore, the analysis of the curve $J(t)$ is a convenient tool to characterize the sample to identify the extreme conditions for the operation of the memory elements, at which the films degrade. Among the works devoted to the study of the effect of pre-polarizing voltage on retention currents, relaxation currents, and $I-V$-dependences in thin-film ferroelectric perovskites based on BFO [10–16], our attention was drawn to the results obtained in Refs. [15,16]. These studies show a strong difference between the electrophysical properties of samples subjected to prolonged ($\sim 900-3600$ sec) exposure to electrical voltage ($\sim 10-15$ V) before measurements from films that were not subjected to such treatment. It is of scientific interest to modify the approach used in Ref. [15], that is, to increase the pre-exposure voltage to several tens of volts, while lowering the voltage application time in the range of $0-5$ sec. The effect of the magnitude ($30-55$ V)

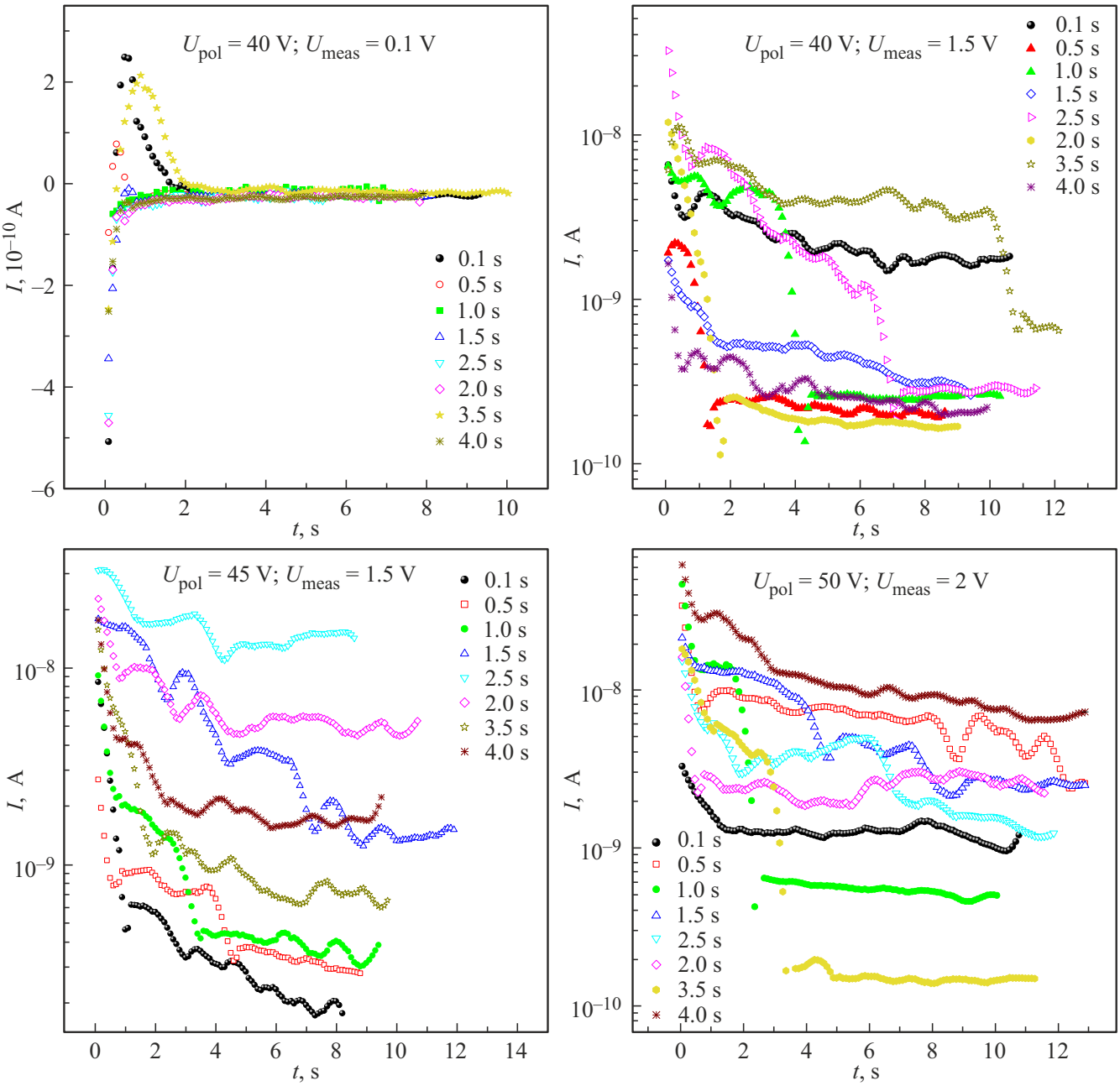

Figure 1. The dynamics of changes in relaxation currents with increasing exposure time (indicated on the right in the frame) of the polarizing voltage and its magnitude after switching the voltage U_{pol} to U_{meas} (indicated on top in the frame), measured at different U_{meas}.

and exposure time (0.1–4 sec) of the pre-polarizing voltage on relaxation currents in the $BiFeO_3/TiO_2(Nt)Ti$ structure is discussed in this paper, measured in the first few seconds after its reset to low measuring voltages characteristic of the operating conditions of memory elements in the range of ~ 0.1–2 V.

2. Samples and experimental procedure

BFO films with a thickness of 50 nm were grown by atomic layer deposition (ALD) on an ALDCERAM ML-200 installation. A titanium plate was used as a substrate, on which $TiO_2(Nt)$ film in the form of vertical nanotubes was previously obtained by electrochemical method. The ALD method makes it possible to obtain films with 100 % conformity, which is relevant for the chosen system. The thickness of the $TiO_2(Nt)$ layer was $\sim 2.0\,\mu$m. $Bi(mmp)_3$ (tris(1-methoxy-2-methyl-2-propoxyvismuth) and ferrocene $Fe(cp)_2$ were used as precursor sources. In ALD method the precursors were delivered to the chamber using a carrier gas N_2 with a purity of 99.999 %. The evaporation temperature range of $Bi(mmp)_3$ was 135–145 °C, and the

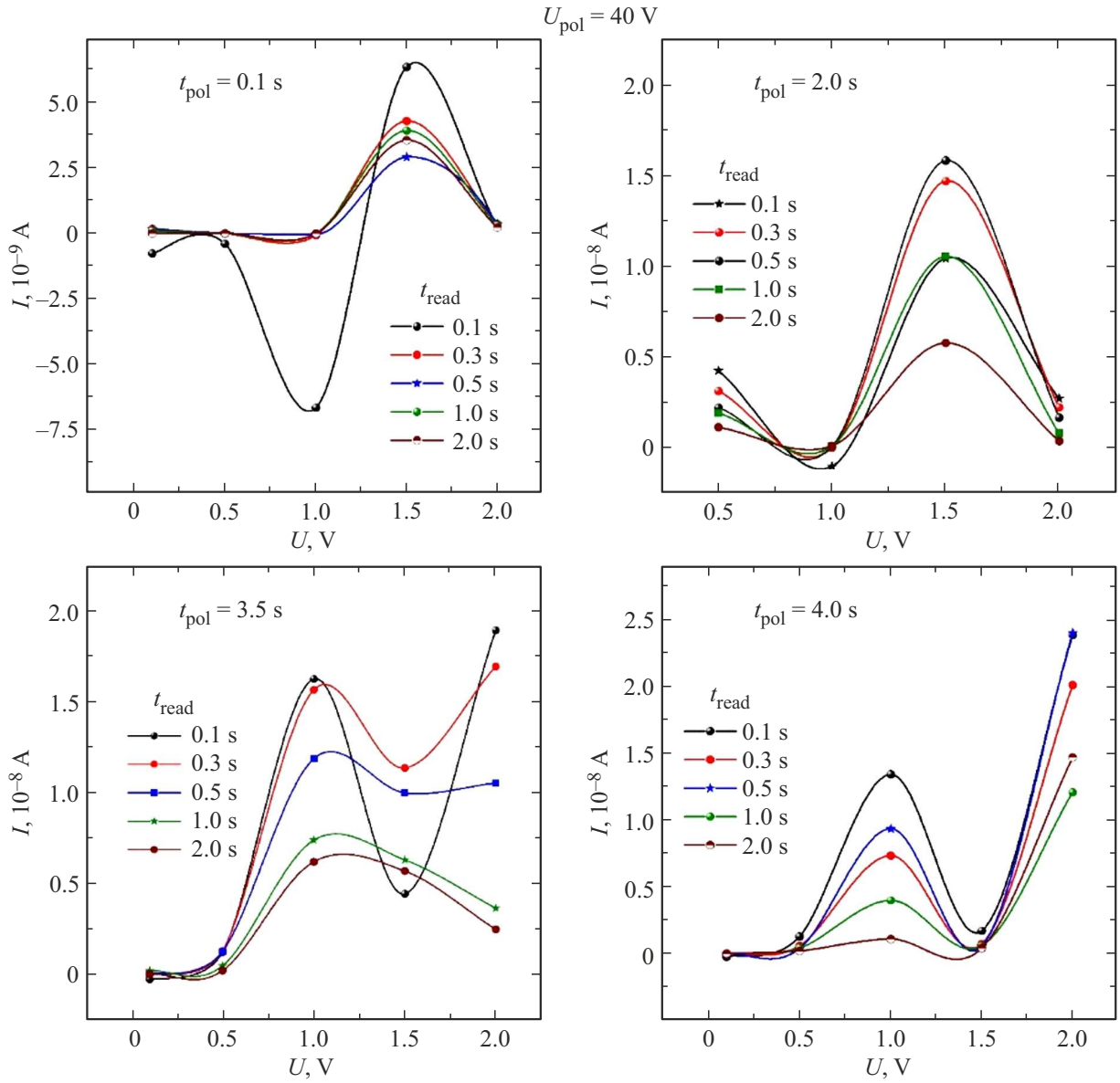

Figure 2. $I-V$-sample dependencies formed for currents after reset $U_{pol} = 40$ V for measuring voltage U_{meas} from the range of 0.1–2 V for different t_{read} and t_{pol}. The time of reading the current t_{read} after resetting U_{pol} to U_{meas} and the time of applying the pre-polarizing voltage t_{pol} are specified in the limits.

evaporation temperature of ferrocene was 90 °C. ALD BiO_x consisted of a $Bi(mmp)_3$ precursor pulse with a duration of 1,2 sec, followed by N_2 admission of pulse of O_3 — 5 sec, in the interval between cycles, nitrogen purging was performed for 15 sec. Then the cycles of ALD FeO_x were applied. Pulse duration of the $Fe(C_5H_5)_2$ precursor — 2 sec. The number of admission subcycles of each precursor was 90. Throughout the entire experiment, the inlet and outlet gas pipelines were maintained at a temperature of 150 °C. The substrate was located at a distance of 4–5 cm from the inlet. The reactor was uniformly heated to 250 °C. Afterwards, the resulting samples were heat treated in air at temperature of 660 °C for 60 min. To carry out electrical measurements, the contacts were deposited on the surface using magnetron sputtering, and a titanium substrate served as the bottom electrode. The experimental part of the fabrication of this structure is described in more detail in paper [8].

Relaxation currents were measured using a Keithley 2400 measuring source. A two-stage voltage of large — U_{pol} (30–55 V) and small — U_{meas} (0.1–2 V) values was applied to the sample. At the same time, the current was not measured during the action of the high step t_{pol} (0.1–4 sec) and it played the role of forming or polarizing the sample. The current measurement took place at the moment of switching steps $U(t)$ from U_{pol} to U_{meas} during the time t_{read} from 0.1 sec to 15 sec. The operation of the measuring source was automated in the LabVIEW environment; the

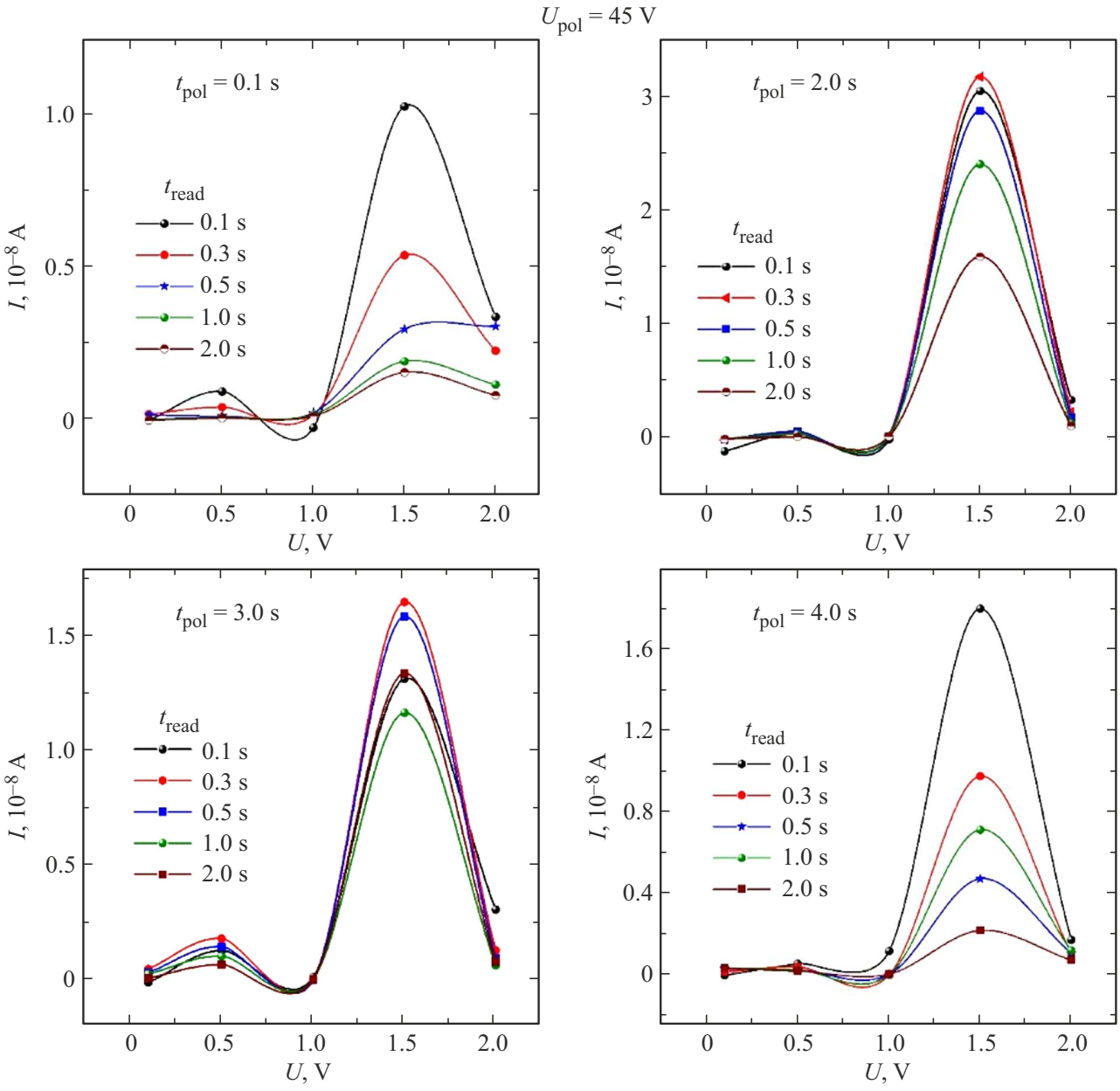

Figure 3. $I-V$-sample dependencies formed for currents after reset $U_{pol} = 45$ V for measuring voltage U_{meas} from the range 0.1–2 V for different t_{read} and t_{pol}. The time of reading the current t_{read} after resetting U_{pol} to U_{meas} and the time of applying the pre-polarizing voltage t_{pol} are specified in the limits.

signal integration time corresponded to one period of mains voltage (1PLC). The upper electrical contact was created by a clamping (spring-loaded) platinum electrode with a diameter of 0.3 mm to which a displacement potential was applied, the lower contact was a titanium substrate with a grounding.

3. Results and discussion

The time dependences of the current after high voltage discharge were studied to analyze the effect of pre-polarization on the dynamics of relaxation processes and the formation of conductivity in the structure of $BiFeO_3/TiO_2(Nt)$ and the corresponding VAC was constructed under various exposure modes U_{pol} and t_{pol}. Figure 1 shows the dynamics of changes in the relaxation of the current $I(t)$ with variations in the magnitude U_{pol} and the exposure time t_{pol} of the polarizing (molding) voltage measured at different values U_{meas}.

The curves $I(t)$ for $U_{meas} = 0.1$ V are characterized by a negative value at the initial moment of time, and later, with the inversion of the sign, they pass through the maximum. This indicates the predominance of the depolarization field directed towards the measuring U_{meas} at the time of reset

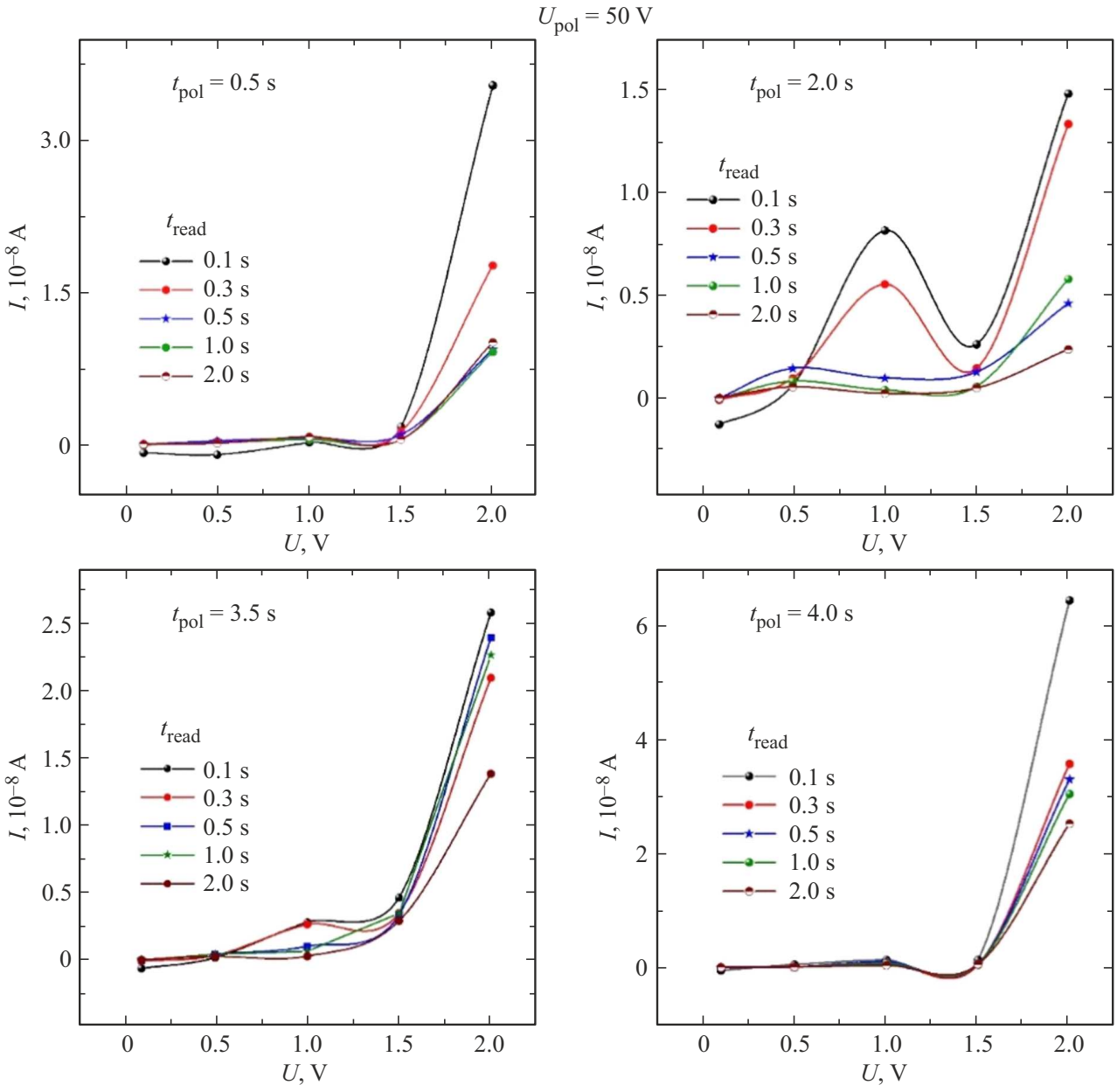

Figure 4. $I-V$-sample dependencies formed for currents after reset $U_{pol} = 50$ V for measuring voltage U_{meas} from the range 0.1−2 V for different t_{read} and t_{pol}. The time of reading the current t_{read} after resetting U_{pol} to U_{meas} and the time of applying the pre-polarizing voltage t_{pol} are specified in the limits.

U_{pol} to U_{meas} [17]. The range of relaxation currents recorded at 1.5 and 2 V covers a corridor of approximately two orders of magnitude for the entire time range of t_{pol}. The dependences $I(t)$ in Figure 1 demonstrate the presence of alternating sections of current decline and rise with a general tendency to relaxation behavior. The decrease and rise of the relaxation curves of the BFO current is interpreted as capture and emptying by charge carriers of deep (impurity) centers in the sample, the role of which is played by positively charged oxygen vacancies $V\ddot{o}$, which inevitably occur at one of the technological stages of manufacturing the film structure [15,16]. In the future, during the presentation of the material, the figures will show the dependencies built on the basis of experimentally obtained data (Figure 1). Figure 2−4 shows the volt-ampere characteristics (VAC) compiled for current values $I(t)$ at U_{meas} from the series 0.1−2 V in 0.5 V increments in the time of reading t_{read} after switching the pre-polarization voltage from U_{pol} to U_{meas} (the magnitude and time of its application t_{pol} are shown in the figures above). VAC dependencies (Figure 2) at the reading time $t_{read} = 0.1$ sec for t_{pol} — 0.1; 0.5; 1 and 1.5 sec pass through two maxima with a sign inversion of I. For other time values, t_{read} VAC are positioned by having a maximum at the abscissa

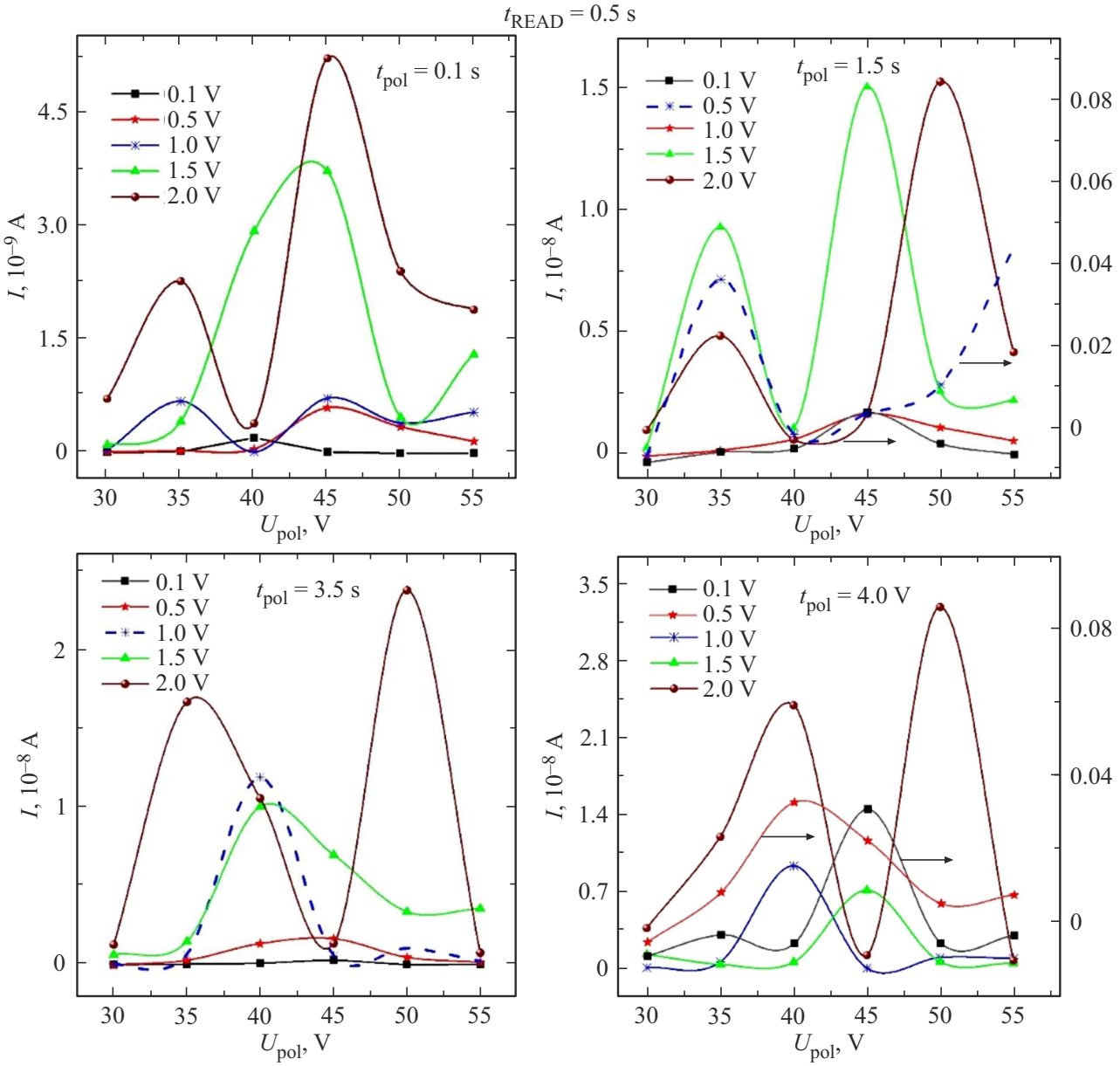

Figure 5. Effect of polarization (forming) voltages U_{pol} on the current at a fixed low voltage, measured over time t_{read} — 0.5 sec after resetting U_{pol} to U_{meas}. The curves were obtained for different times t_{pol}.

point — 1.5 V except when t_{pol} are 3.5 and 4 sec, where VAC are N-shaped. In the case of a pre-polarization voltage of 45 V (Figure 3) $I(U)$, the dependences illustrate pronounced maxima in the vicinity of 1.5 V starting from $t_{pol} = 0.5$ sec, and for $U_{pol} = 50$ V (Figure 4) the graphs represent an exponential dependence of $I(U)$ except in the case of $t_{pol} = 2$ sec, where there are differenly manifested N-shaped VAC.

In order to facilitate visual perception of the effect of the pre-voltage U_{pol} and the time of its effect t_{pol} on relaxation currents at various values U_{meas}, the dependences shown in Figure 5 are constructed. The graphs in Figure 5 correspond to relaxation currents at a fixed low voltage, measured after the time $t_{read} = 0.5$ sec after switching the pre-high voltage to a low measuring one. It can be seen from Figure 5 that the maximum values of relaxation currents are reached at measuring voltages 1.5 and 2 V, pretreated with voltages 45 and 50 V for almost the entire exposure time range t_{pol}. The effect of time t_{pol} on relaxation currents at the above parameters can be traced in Figure 6, which indicates the ambiguous behavior of the current with variations in the voltage holding time U_{pol}. Curve $I(t_{pol})$ with parameters: $U_{meas} = 1.5$ V; $t_{read} = 0.1$ sec; for $U_{pol} = 45$ V has a maximum in the region of ~ 2 sec, which is modified into a doublet structure with a decrease in current along the entire curve when increasing U_{pol} to 50 V. For t_{read} equal

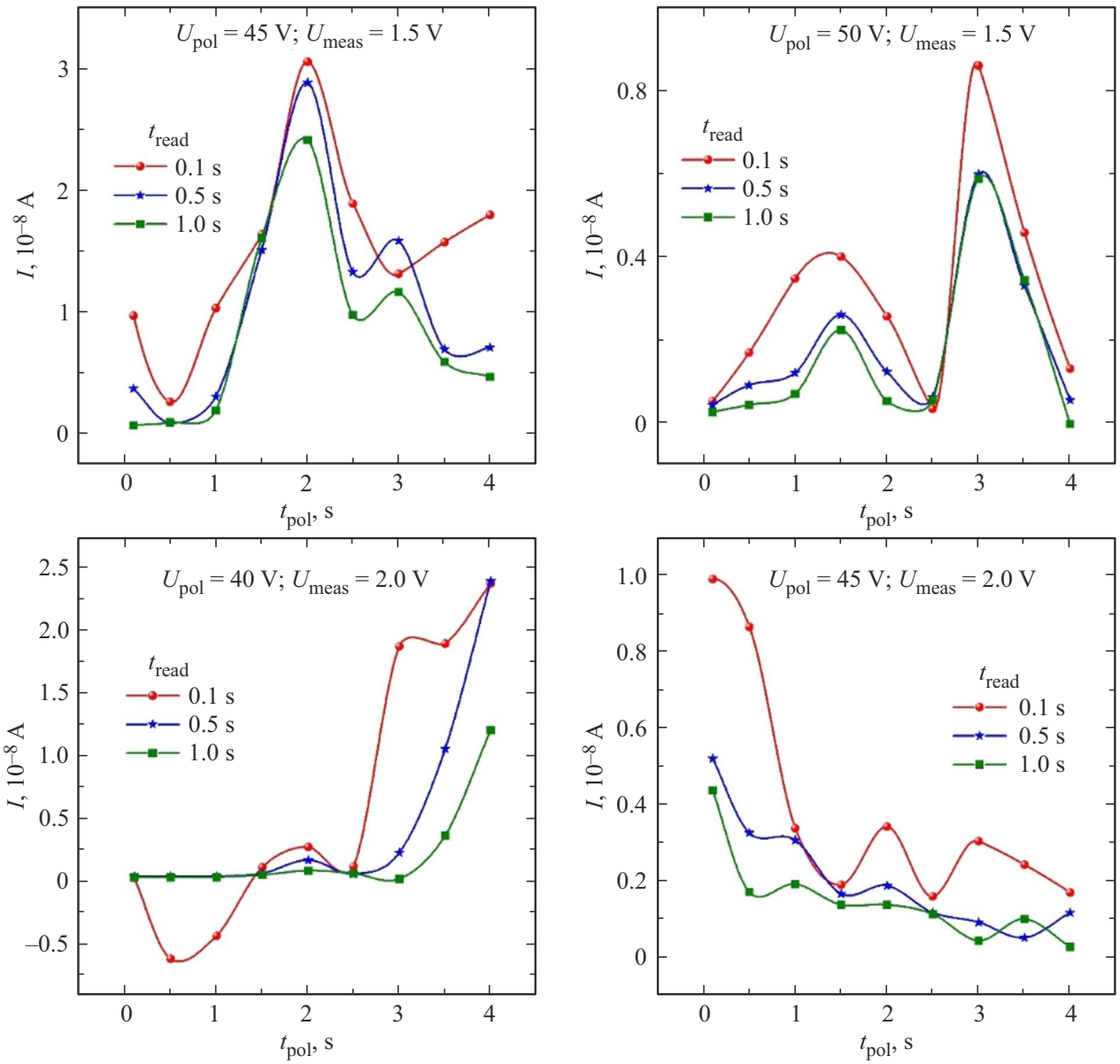

Figure 6. The effect of exposure time t_{pol} of the pre-polarization voltage U_{pol} on relaxation currents at a fixed low measuring voltage U_{meas}. The values of the corresponding values are indicated in the frames above the graphs.

to 0.5 and 1 sec the doublet structure $I(t_{pol})$ undergoes a change in the ratio of short-term and long-term maxima towards an increase in the latter when voltage is applied $U_{pol} = 50$ V. The currents measured at 2 V for U_{pol} — 40 and 45 V show the opposite picture: with increasing exposure time $U_{pol} = 40$ V, the current values increase, and for $U_{pol} = 45$ V — on the contrary, the dependencies $I(t_{pol})$ are falling with a weak oscillation. Curves $I(t_{pol})$ for the case of $U_{pol} = 50$ V pass through a wide maximum in the initial section of the dependence, while the current increases noticeably for all curves.

Previously, we demonstrated the memristive properties of the studied samples [9], which, in most cases, are caused by the appearance and destruction of conductive filaments as a result of molding stress. Figure 7 shows the VAC from the resulting structure, which confirms the memristive behavior. From this point of view, it is acceptable to assume that the growth of the curves $I(t_{pol})$ for $U_{pol} = 40$ V and $U_{meas} = 2$ V (Figure 6) is associated with the formation of a conductive channel with a relatively long ($t_{pol} > 2$ sec) when exposed to pre-polarization voltage, and a decrease in leakage currents in the case of $U_{pol} = 45$ V — partial destruction of filaments during prolonged exposure to molding voltage.

Schottky field emission and spatial charge-limited currents (SCLC) are among the main mechanisms of electric charge transfer in the metal-dielectric(semiconductor)-metal (MDM) structure. The Schottky emission equation is given

Parameters of the SCLC structure $BiFeO_3/TiO_2(Nt)Ti$

U_{pol}, V	U_{TFL}, V	t_{pol}, sec	R, Om	RC, sec	σ, $Om^{-1}m^{-1}$	$\varepsilon\varepsilon_0$, F/m	N_t, m^{-3}
40	0.5	3.5	$6 \cdot 10^7$	$3 \cdot 10^{-3}$	$0.43 \cdot 10^{-7}$	$1.29 \cdot 10^{-10}$	$0.19 \cdot 10^{21}$
45	1.0	4	$8.3 \cdot 10^7$	$4.1 \cdot 10^{-3}$	$0.32 \cdot 10^{-7}$	$1.29 \cdot 10^{-10}$	$0.38 \cdot 10^{21}$
50	1.5	3.5	$8 \cdot 10^7$	$4 \cdot 10^{-3}$	$0.33 \cdot 10^{-7}$	$1.3 \cdot 10^{-10}$	$1.2 \cdot 10^{21}$

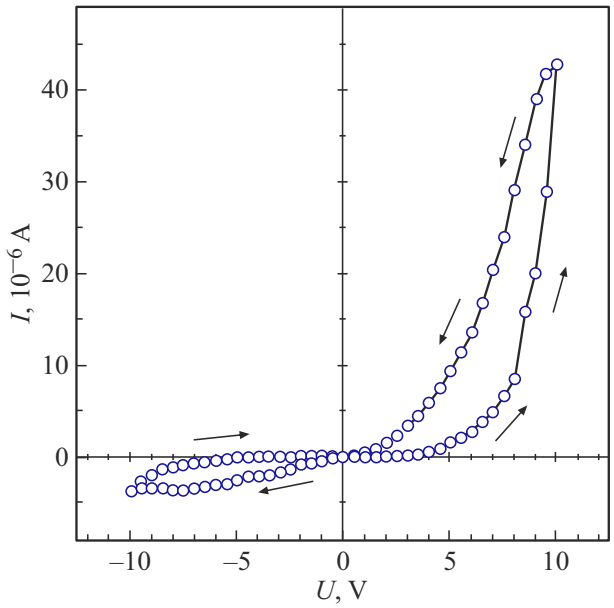

Figure 7. VAC of $BiFeO_3/TiO_2(Nt)Ti$ structure, memristive behavior.

by the following expression [18]:

$$J_s = AT^2 \exp\left[\frac{W_b}{kT} - \frac{1}{kT}\left(\frac{q^3 V}{4\pi\varepsilon\varepsilon_0 d}\right)^{1/2}\right], \qquad (1)$$

where A is the Richardson's constant, W_b is the height of the potential barrier without taking into account its lowering by electric image forces, ε is the dielectric constant of the film material in the optical region, ε_0 — dielectric constant, d — film thickness, V — external voltage, q — unit of charge, k — Boltzmann constant, T — temperature.

An analysis of the most typical exponential curves (Figure 4, $t_{pol} = 3.5$ sec) plotted in Schottky coordinates $\ln(I) - E^{1/2}$, Poole-Fraenkel coordinates $\ln(I/E) - E^{1/2}$ and SCLC $\ln(I) - \ln(E)$ showed that these dependencies are better A straight line is approximated for the Schottky and SCLC mechanism (Figure 8). For the case of 40 V prestress, the ascending branch of the maximum of the VAC in Figure 2 ($t_{pol} = 3.5$ sec) is better approximated by a straight line in the coordinates of the SCLC. This indicates the joint participation of Schottky and SCLC mechanisms in the conductivity of the studied samples.

The voltage of a sharp increase in the VAC current during prolonged ($t_{pol} > 3$ sec) exposure to the pre-polarizing voltage (Figure 2) shifts from 0.5 V to 1 V (Figure 3) and up to 1.5 V (Figure 4) with an increase in the magnitude of the pre-polarizing step, the voltage applied to the sample $U(t)$. Developing the idea described in Ref. [15] on the accumulation of positively charged oxygen vacancies at the cathode as a result of their movement in the direction of the electric field, it is logical to assume that an increase in the duration of action and the magnitude of the pre-voltage should lead to an increase in the concentration of oxygen vacancies in the cathode region of TiO_2.

With the SCLC mechanism, the voltage of a sharp increase in the current at the VAC — U_{TFL} is associated with the concentration of electron capture traps N_t (in our case — oxygen vacancies) the ratio [19]:

$$U_{TFL} = \frac{qN_t d^2}{2\varepsilon\varepsilon_0}. \qquad (2)$$

To find $\varepsilon\varepsilon_0$, we used the Maxwell relaxation time $\tau = RC = \varepsilon\varepsilon_0/\sigma$; The values of R were determined in the VAC maxima (Figures 2–4) for the duration of the application U_{pol} greater than 3 sec. Using the following parameters: film thickness $d = 2.05 \cdot 10^{-6}$ m; electrode area $S = 0.78 \cdot 10^{-6}$ m^2; electrical capacity $C = 10$ pF were calculated N_t from (2) for the cases pre-voltage 40 V, 45 V and 50 V. The calculation results are shown in the table.

As can be seen from the table, an increase in the pre-exposure voltage leads to an increase in Nt. Taking into account the above, the features of the VAC in the form of maxima in Figures 3 and 4 can be explained as follows: at low levels of electron injection (low voltages), as their impurity centers capture, the number of injected current carriers involved in conduction increases (ascending branch of the maximum); with a further increase in voltage (high level electrons are trapped at deeper levels (cluster *Vö*), while the lifetime of newly injected charge carriers increases as the traps are occupied. In a situation where the lifetime of the injected electrons is longer than the Maxwell relaxation time, a spatial charge occurs at the cathode that limits further current (the descending branch of the VAC maximum).

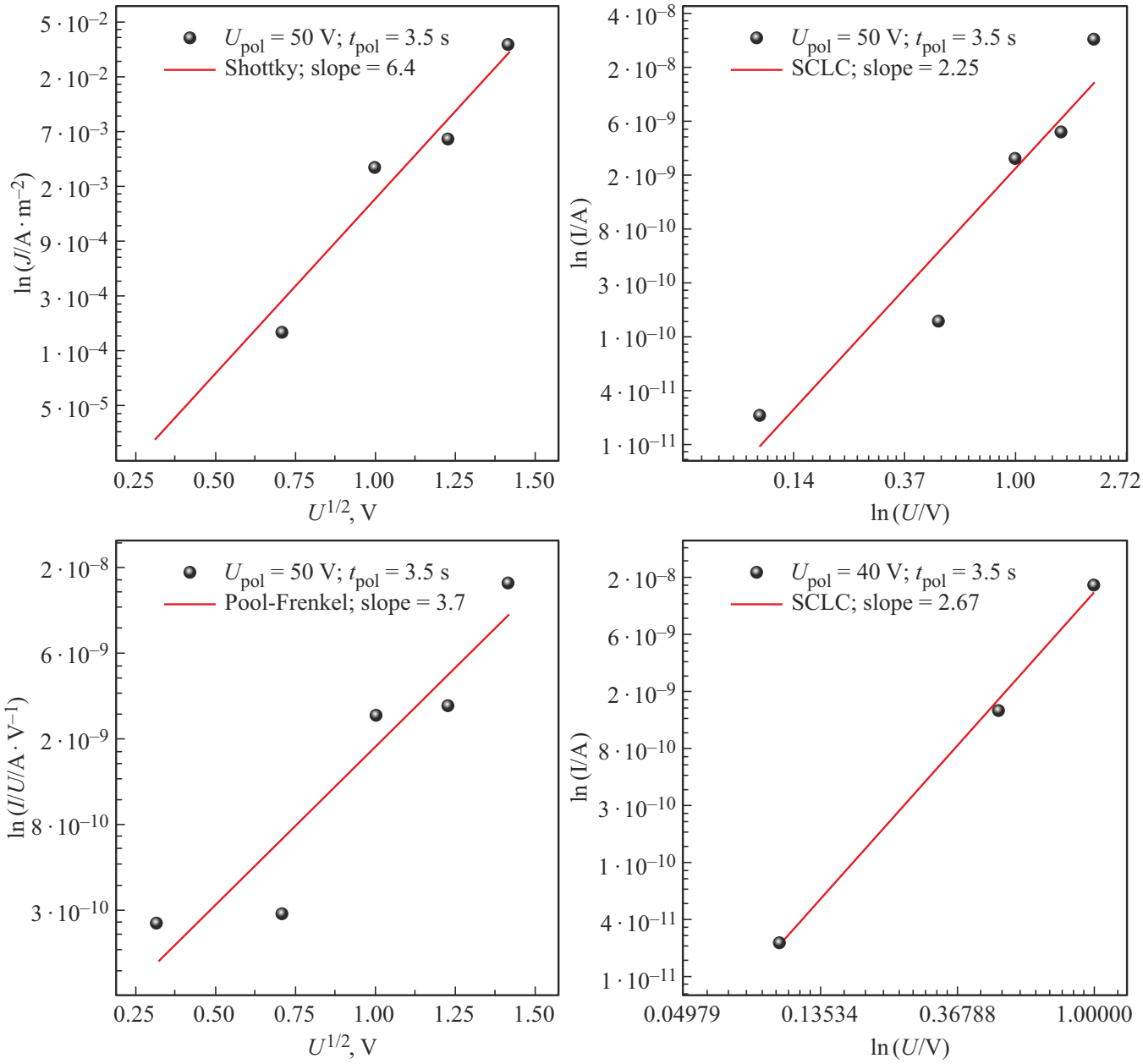

Figure 8. VAC of the sample in Schottky, SCLC, and Poole-Fraenkel coordinates under the conditions of external influence indicated above in the framework. The slope coefficients of the fitting lines are given near the names of the conduction mechanism.

Conclusion

Thus, the analysis of relaxation currents after resetting the pre-polarizing voltage U_{pol} in the range of 30−55 V and various exposure times (0.1−4 sec) showed that the VAC of the $BiFeO_3/TiO_2$(Nt)Ti structure at low measuring voltages (0.1−2 V) exhibit pronounced non-monotonic features in the form of maxima $I(U)$ and N-shaped sections. It is established that these features are caused by the drift and accumulation of oxygen vacancies in the cathode region during the pre-polarization process, which changes the local conditions of carrier injection and capture. The analysis of the dependencies in the Schottky, Poole-Fraenkel coordinates and the current limited by the spatial charge showed the dominant participation of the Schottky and SCLC mechanisms in the formation of the conductivity of the structure after the reset U_{pol}. The estimated increase in the trap concentration with an increase in the magnitude of the preliminary stress confirms the relationship between the dynamics of defects and the observed relaxation behavior. The results obtained demonstrate the fundamental possibility of controlling the conductivity and state of the $BiFeO_3/TiO_2$(Nt)Ti memristive structure by means of controlled electrical pre-polarization, which is of interest for

optimizing operating modes and increasing the reliability of oxide memristors.

Conflict of interest

The authors declare that they have no conflict of interest.

References

[1] D.B. Strukov, G.S. Snider, D.R. Stewart, R.S. Williams. Nature **453**, 80–83 (2008).
[2] J. Borghetti, G.S. Snider, P.J. Kuekes, J.J. Yang, D.R. Stewart, R.S. Williams. Nature **464**, 873–876 (2010).
[3] J. Yang, D.B. Strukov, D.R. Stewart. Nature Nanotechnology **8**, 13–24 (2013).
[4] A.Q. Jiang, C. Wang, K.J. Jin, X.B. Liu, J.F. Scott, C.S. Hwang, T.A. Tang, H.B. Lu, G.Z. Yang. Advanced Materials **23**, 1277–1281 (2011).
[5] Z. Zhao, A. Abdelsamie, R. Guo, S. Shi, J. Zhao, W. Lin, K. Sun, J. Wang, J. Wang, X. Yan, J. Chen. Nano Research **15**, *3*, 2682–2688 (2022).
[6] J. Wu, J. Wang. Journal of Applied Physics **108**, 094102 (2010).
[7] J. Wu, X. Lou, Y. Wang, J. Wang. Electrochemical and Solid-State Letters **13**, G9–G11 (2009).
[8] F. Orudzhev, S. Ramazanov, D. Sobola, A. Isaev, C. Wang, A. Magomedova, M. Kadiev, K. Kaviyarasu. Nanomaterials **10**, 2183 (2020).
[9] S. Ramazanov, F. Orudzhev, G. Gajiev, V. Holcman, R.S. Matos, H.D. da Fonseca Filho, S. Tălu, D. Selimov. Applied Surface Science **158863** (2023).
[10] M.-T. Chentir, E. Bouyssou, L. Ventura, C. Anceau. Journal of Applied Physics **105**, 061605 (2009).
[11] A.Q. Jiang, C. Wang, K.J. Jin, X.B. Liu, J.F. Scott, C.S. Hwang, T.A. Tang, H.B. Lu, G.Z. Yang. Advanced Materials **23**, 1277–1281 (2011).
[12] Y. Podgorny, K. Vorotilov, A. Sigov. AIP Advances **6**, 095025 (2016).
[13] Yu.V. Podgorny, A.N. Antonovich, K.A. Vorotilov, A.S. Sigov. Ferroelectrics **544**, 82–87 (2019).
[14] S. Lancaster, P.D. Lomenzo, M. Engl, B. Xu, T. Mikolajick, U. Schroeder, S. Slesazeck. Frontiers in Nanotechnology **4**, 939822 (2022).
[15] H. Zhu, Y. Yang, X. Meng, A. Jiang, Z. Bai, X. Zheng, L. Jin, C. Wang, S. Feng. Applied Physics Letters **112**, 182904 (2018).
[16] Y. Yang, H. Zhu, D. Chu, K. Liu, Y. Zhang, M. Pei, S. Feng, L. Jin, C. Wang, J. Liu, R. Li, S. Wang. Journal of Physics D: Applied Physics **53**, 115301 (2020).
[17] G.M. Gadzhiev, Sh.M. Ramazanov, N.S. Abakarova, T.N. Efendieva. FTT, **66** (2), 259–265 (2024) (in Russian).
[18] V.L. Bonch-Bruevich, S.G. Kalashnikov. Fizika poluprovodnikov, Nauka, M. (1977) (in Russian).
[19] F.-C. Chiu. Advances in Materials Science and Engineering **2014**, 578168 (2014).

Translated by A.Akhtyamov